MODELING CONTOURED TRAILING EDGE FLAP CONTROLS

Y. K. Yillikçi[†]
Istanbul Technical University,
80626 Maslak, Istanbul, TURKIYE

S. Hanagud[‡]
Georgia Institute of Technology,
Atlanta, GA 30332-1500 USA

Abstract

A simplified trim procedure coupled with a nonlinear partial differential equation solver is developed for calculating elastic blade tip deflections of rotor blades with contoured trailing edge flap controls. Flap deflections are modeled up to second harmonics and different sinusoidal flap shapes. Forward flight steady-state flight conditions of a test in flight model helicopter are calculated by a set of vehicle trim equations. A conditionally stable explicit finite difference scheme is used to numerically integrate the nonlinear P.D.E's of motion in space and time to obtain the aeroelastic transient response of a hingeless rotor blade with trailing edge flap control. New aerodynamic environment due to flap control is formulated based on Theodorsen's unsteady oscillating airfoil aerodynamics representation including preiodic trailing edge flap motions. Transient and state blade tip deflections are calculated for the selected model helicopter configuration including different flap contours and blade stiffnesses.

Nomenclature

$C_{T_{MR}}$	main rotor thrust coeff. $\frac{T_{MR}}{\rho\pi R^4\Omega^2}$	C_W	weight coeff. $\frac{W}{\rho\pi R^4\Omega^2}$
L_v, L_w	lift in v and w directions,	M_ϕ	aerodynamic moment
v, w	blade elastic deflections	U_P, U_T	velocity components
γ	Lock number	λ_0	rotor induced uniform inflow
$\Lambda_0, \Lambda_{1s}, \Lambda_{1c}$	flap control inputs	μ	advanced ratio, $\frac{V}{\Omega^2 R}$
σ	blade solidity, $\frac{bc}{\pi R}$	ϕ	elastic twist (rad)
ψ	azimuth angle	Ω	rotor speed (rad/sec)

I. Introduction

Flap Controlled Rotor Blade Concept

The use of swash-plate systems for applying collective and cyclic pitch change has been the primary element of helicopter controls since the earlier phases of its development. Almost today's all rotorcrafts involve swash-plate system as the main control device for adjusting the blade pitch angle in order to balance aerodynamic lift and moment distribution. The application of trailing edge flaps to manipulate rotor blade lift variation was first introduced by Charles Kaman, a distinguished helicopter pionner, and the concept called *servo-flap* was successfully used in several Kaman helicopters.

A new decade in helicopter performance, comfort and agility is expected to be achieved by the implementation of rotor active control technology. But the break through of this technology is still missing due to lack of appropriate rotating blade actuation systems.

---

† Asst. Prof, Faculty of Aeronautics and Astronautics

‡ Professor, CERWAT and School of Aerospace Engineering

Smart materials are expected to open new possibilities for the realisation of rotor active control. At this point the only applicable blade actuation system for individual blade control seems to be a hinged flap application at the outer third of the blade for a conventional size helicopter.

For helicopter rotors the use of trailing edge flaps on the blades has found use only for 1/rev. cyclic pitch contorl, e.g. the Kaman servo-flap. On the other hand, with the newly developing smart materials/structures and high bandwidth active control technologies, it is now becoming increasingly feasible to use compliant airfoil surfaces or trailing edge mounted flaps on rotor blades as a means of individual blade control (IBC). Coupled with real time adaptive feedback strategies, active controlling of the blade lift distribution offers several possibilities for the improvement of the rotor performance, as well as for the reduction of blade loads and vibrations.

With the development of advanced sensors, actuators, command-control systems and demand for new technologies for blade control mechanisms; flap and servo-flap control concepts have been started to be analyzed with new objectives. Recent studies about practical applications of smart structures and materials in helicopter active control has been reviewed by Strehlow [1].

Possible applications of flap controlled rotor systems for Army's High Maneuverability/Agility Rotor Control System (HIMARCS) and conceptual designs of Kaman, Bell and McDonald Douglas (MDHC) helicopter companies have been evaluated detailly in references [2, 3, 4] respectively.

Additional control parameters introduced by flap controls expected to give designers additional flexibilities in tailoring aeroelastic and aerodynamic characteristics of next century's rotor blades. With multi-input flap controls located at outboard section of the blade more efficient blade controls can be achieved with smaller control surfaces. With these expectations complete replacement of standart pitch control with flap control particularly for a 700 lb micro-helicopter configuration is evaluated and periodic response of an elastic rotor blade with flap control have been analyzed by Yillikci [5]. Tip deflections of the flap controlled elastic blade have been compared with the identical pitch controlled blade. Periodic response characteristics of both control cases are found to be almost identical except for the elastic twist which was obtained higher for the flap controlled blade.

II. Formulation

Formulation of aeroelastic analysis of rotor blades with flap controls is consisted of three major steps. First step of the problem is the formulation and calculation of flap control trim settings for the chosen helicopter configuration. The second step of is the formulation of new aerodynamic environment around the rotor blade. The new set of rotor blade nonlinear partial differential equations are solved numerically as the third step.

Trim Formulations

Rotor slowing down transition mode for the stopped rotor requires a different approach for trim formulation. Since slowing main rotor can no longer maintain the total lift required either a descending and slowing down flight condition or utilization of auxiliary lift and forward propulsion are required to keep the aircraft on its steady flight path. All of these conditions are included to the problem whereas the effects of nonuniform blade geometries are considered.

Required trim parameters for the stopped rotor utilized with flap controls are calculated by an approximate trim formulation. Trim conditions for the pitch control case with the same blade and vehicle configuration are first calculated by the use of standart trim equations given by Johnson [10]. As the second step trim parameters directly related with flap control case are recalculated along with the replacement of pitch control with flap control represented up to second harmonics as;

$$\begin{aligned}\Lambda(\xi,\psi) &= \sum_{1}^{k}\left\{S_{ns}\sin\frac{n\pi\xi}{L_f}+S_{nc}\frac{n\pi\xi}{L_f}\right\} \\ &\quad \{\Lambda_0+\Lambda_{tw}\ r+\Lambda_{1s}\sin\psi+\Lambda_{1c}\cos\psi\ +\Lambda_{2s}\sin 2\psi+\Lambda_{2c}\cos 2\psi\} \qquad (1)\end{aligned}$$

where Λ_0 is the collective flap Λ_{tw} is the flap pre-twist, and $\Lambda_{1s}, \Lambda_{1c}, \Lambda_{2s}$ and Λ_{2c}, are first and second harmonics give 1/rev and 2/rev variations of the blade trailing edge flap angle.

Sectional blade lift for two-dimensional strip type aerodynamic formulation is written as;

$$\frac{F_Z}{\sigma a}=\frac{1}{2}\left[U_T^2\theta_{ri}-U_PU_T\right]+\left[\frac{c}{4a}(f_2-f_3)U_T\ \overset{*}{\Lambda}-\frac{c^2}{8a}f_4\ \overset{**}{\Lambda}+\frac{1}{a}f_1U_T^2\Lambda\right] \qquad (2)$$

where θ_{ri} is the rigid pitch angle of the blade, c is the non-dimensional blade chord, Λ is the trailing edge flap angle given by equation 1, a blade lift curve slope and σ is the blade solidity ratio. Parameters f_1, f_2, f_3 and f_4 are related with flap hinge offset geometry which have been introduced by Theodorsen's two-dimensional unsteady aerodynamic formulation for the oscillating airfoils. Detailed expressions of these parameters are given in reference [5].

First term in F_Z formulation is related with blade profile lift with a rigid pitch angle θ_{ri}. Blade sectional velocities U_T and U_P are given in nondimensional form for a rigid blade with only rigid blade flapping motion;

$$U_T=r+\mu\sin\psi$$

$$U_P=\lambda+\overset{*}{\beta}\ r+\beta\mu\cos\psi$$

Resultant blade cross-sectinal velocity is approximated as $U=U_T$. Mean of the total rotor thrust formulated the use of equation 2 as,

$$\begin{aligned}\frac{C_{T_0}}{\sigma a} &= \frac{1}{2}\left(C_{12}+C_{10}\frac{\mu^2}{2}\right)\theta_{ri}-\frac{1}{2}C_{11}\lambda+\left(d_{3k2}+d_{3k0}\frac{\mu^2}{2}\right)\Lambda_0 \\ &+ \left(d_{3k3}+d_{3k1}\frac{\mu^2}{2}\right)\Lambda_{tw}+d_{3k1}\mu\Lambda_{1s}-d_{1k0}\frac{\mu}{2}\Lambda_{1c}-d_{3k0}\frac{\mu^2}{4}\Lambda_{2c} \qquad (3)\end{aligned}$$

Parameters $C_{10}, C_{11}, ..., d_{3k3}$ are related with blade chord and flap geometries and are given in reference [5]. Equation 3 gives the amount of Λ_0 control input required to maintain the mean of the rotor thrust C_{T_0}.

Rotor blade flapping dynamic equilibrium must be also considered to calculate the required cyclic flap angle inputs Λ_{1s}, Λ_{1c} zeroth harmonic of blade flapping, β_0. Flapping dynamics of a rigid rotor can be written as;

$$\overset{**}{\beta}+\nu^2\ \beta=\frac{1}{2}\frac{\rho caR^4}{I_b}\int_0^1 rF_Z dr \qquad (4)$$

where blade flapping motion is expressed as up to its first harmonics,

$$\beta = \beta_0 + \beta_{1s}\sin\psi + \beta_{1c}\cos\psi \tag{5}$$

Harmonic balance of equation 4 up to its second harmonics gives five equilibrium conditions as;

$$\frac{\nu^2}{\gamma}\beta_0 - \left(d_{3k3} + d_{3k1}\frac{\mu^2}{2}\right)\Lambda_0 + C_{12}\frac{\lambda}{2} - \left(d_{3k4} + d_{3k2}\frac{\mu^2}{2}\right)\Lambda_{tw} - \left(\frac{C_{13}}{2} + C_{11}\frac{\mu^2}{4}\right)\theta_{ri} + d_{1k1}\frac{\mu}{2}\Lambda_{1c} - d_{3k2}\,\mu\Lambda_{1s} + d_{3k1}\frac{\mu^2}{4}\Lambda_{1c} \tag{6}$$

$$-2\,d_{3k2}\,\mu\,\Lambda_0 - \left(d_{2k1} + d_{3k1}\frac{3\mu^2}{4} + d_{3k3}\right)\Lambda_{1s} + d_{1k2}\,\Lambda_{1c} + d_{1k1}\,\mu\Lambda_{2s} + d_{3k2}\,\mu\Lambda_{2c} + \left(C_{11}\frac{\mu^2}{8} - \frac{C_{13}}{2}\right)\beta_{1c} + \frac{(\nu^2-1)}{\gamma}\beta_{1s} - 2\,d_{3k3}\,\mu\,\Lambda_{tw} - C_{12}\,\mu\,\theta_{ri} + \frac{1}{2}C_{11}\mu\lambda = 0 \tag{7}$$

$$-d_{1k2}\,\Lambda_{1s} - \left(d_{2k1} + d_{3k1}\frac{\mu^2}{4} + d_{3k3}\right)\Lambda_{1c} + d_{1k1}\mu\Lambda_{2s} + d_{3k2}\mu\Lambda 2c + C_{12}\frac{\mu}{2}\beta_0 + \left(C_{11}\frac{\mu^2}{8} + \frac{C_{13}}{2}\right)\beta_{1s} + \frac{(\nu^2-1)}{\gamma}\beta_{1c} = 0 \tag{8}$$

$$d_{3k1}\frac{\mu^2}{2}\Lambda_0 + d_{3k2}\mu\Lambda_{1s} - d_{1k1}\frac{\mu}{2}\Lambda_{1c} - 2d_{1k2}\Lambda_{2s} - \left(4d_{2k1} + d_{3k1}\frac{\mu^2}{2} + d_{3k3}\right)\Lambda_{2c} + C_{12}\frac{\mu}{2}\beta_{1c} + d_{3k2}\frac{\mu^2}{2}\Lambda_{tw} + C_{11}\frac{\mu^2}{4}\theta_{ri} = 0 \tag{9}$$

$$-d_{1k1}\frac{\mu}{2}\Lambda_{1s} + d_{3k2}\mu\Lambda_{1c} + 2d_{1k2}\Lambda_{2c} - \left(4d_{2k1} + d_{3k1}\frac{\mu^2}{2} + d_{3k3}\right)\Lambda_{2s} + C_{12}\frac{\mu}{2}\beta_{1s} + C_{11}\frac{\mu}{4}\beta_0 = 0 \tag{10}$$

Aerodynamic Formulation

The nonconservative generalized forces which come as a result of the aerodynamic environment are presented in this section. In present formulation, the aerodynamic terms are determined by from Greenberg's extension of Theodorsen's theory as presented in reference [11] for thin, two-dimensional airfoils undergoing unsteady motion in a time-varying incompressible free-stream. As formulated in references [11, 13]. Theodorsen theory faciliates chordwise rigid airfoil with aerodynamically unbalanced trailling edge flap or control surface hinged at $x = \frac{c}{2}c_{cf}$. The airfoil may have move in vertical translation $h(t)$ and rotate about an axis at $x = \frac{c}{2}a$ through an angle $\alpha(t)$; $\Lambda(t)$ donates the angular displacement of the flap relative to the chordline of the airfoil. The positive direction of these variables are as illustrated in Figure 1.

A quasi-steady aerodynamic approximation is employed wherein Theodorsen's lift deficiency function $C(k)$ is taken as equal to unity. The circulatory and noncirculatory lift

and moment per unit span, assuming pitch occurs about the quarter chord can be written based on the derivation given in reference [11] where circulatory and noncirculatory lift components are derived as;

$$L_C = \frac{1}{2}\rho acU\left[-U_P + \frac{c}{2}\dot{\alpha}\right] + \rho cU\left[U\Lambda f_1 + \frac{c}{4}\dot{\Lambda} f_2\right] \tag{11}$$

$$L_{NC} = \frac{1}{2}\rho a\frac{c^2}{4}\left[-\dot{U}_P + \frac{c}{4}\ddot{\alpha}\right] \; - \; \rho\frac{c^2}{4}\left[U\dot{\Lambda} f_3 + \frac{c}{2}\ddot{\Lambda} f_4\right] \tag{12}$$

and the sectional aerodynamic pitching moment is also expressed as,

$$\begin{aligned} M_\phi = \frac{1}{2}\rho a\frac{c^3}{16}\left[\dot{U}_P - U\dot{\alpha} - \frac{3c}{8}\ddot{\alpha}\right] \; &- \; \frac{1}{4}\rho a\frac{c^3}{4\pi}\left[U\dot{\Lambda}\left(\frac{f_2}{2} + f_7\right) + \frac{c}{2}\ddot{\Lambda} f_8\right] \\ &+ \; \frac{1}{2}\rho a\frac{c^2}{4\pi}\left[-U^2\Lambda(f_1 + f_3)\right] \end{aligned} \tag{13}$$

Specifically for the rotary wing aerodynamic representation, U_P is related to $\dot{h}$ and $U\alpha$ in reference [12]as

$$U_P \cong -(\dot{h} + U\alpha)$$

The total velocity, U is the resultant of vertical and tangential velocities as

$$U^2 = U_T^2 + U_P^2$$

U_T and U_P are given in nondimensional form in terms of the elastic variables, spanwise and azimuthal location, pitch, inflow ratio, rotor rotational velocity and advance ratio as,

$$U_T = \overset{*}{v} + (x + \mu\sin\psi) + \mu v^+\cos\psi \tag{14}$$

$$\begin{aligned} U_P \; &= \; \overset{*}{w} - \mu(\theta + \phi)v^+\cos\psi + \mu(w^+ + \beta_{pc})\cos\psi - \lambda + (w^+ v + v\beta_{pc}) - \overset{*}{v}(\theta + \phi) \\ &- \; (\theta + \phi + v^+ w^+)(x + \mu\sin\psi) \end{aligned} \tag{15}$$

Finally the lift components in lead-lag and flap directions are expressed in terms of the circulatory and noncirculatory lift components in reference [13] as

$$L_v \; = \; -(\theta + \phi)\left(L_C\cos\varrho + L_{NC} - D\sin\varrho\right) + \left(-L_C\sin\varrho - D\cos\varrho\right) \tag{16}$$

$$L_w \; = \; \left(L_C\cos\varrho + L_{NC} - D\sin\varrho\right) - (\theta + \phi)\left(L_C\sin\varrho + D\cos\varrho\right) \tag{17}$$

where the airfoil sectional drag is approximated as

$$D = \frac{1}{2}\rho cC_{D0}U^2$$

with the geometric relations illustrated in Figure 2,

$$\sin\varrho = \frac{U_P}{U}, \quad \cos\varrho = \frac{U_T}{U}$$

the lift components are writeen in nondimensional form as

$$L_v = \frac{\gamma}{6}\left\{\left[U_P^2 - \frac{c}{2}U_P\ \overset{*}{\alpha}\right] + \frac{C_{D0}}{a}\left[U_T U_P(\theta+\phi) - U_T^2\right] + (\theta+\phi)\left[U_T U_P - \frac{c}{2}U_T\ \overset{*}{\alpha} + \frac{c}{4}\ \overset{*}{U_P}\right]\right.$$
$$- \frac{2}{a}\left[U_P U_T \Lambda f_1 + \frac{c}{4}U_P\ \overset{*}{\Lambda}\ f_2\right] - \frac{2}{a}(\theta+\phi)\left[U_T^2\Lambda f_1 + \frac{c}{4}U_T\ \overset{*}{\Lambda}\ f_2\right]$$
$$\left. + (\theta+\phi)\frac{c}{2a}\left[U_T\ \overset{*}{\Lambda}\ f_3 + \frac{c}{2}\ \overset{**}{\Lambda}\ f_4\right]\right\} \tag{18}$$

$$L_w = \frac{\gamma}{6}\left\{\left[-U_P U_T + \frac{c}{2}U_T\ \overset{*}{\alpha} - \frac{c}{4}\ \overset{*}{U_P}\right] - (\theta+\phi)\left[-U_P^2 + \frac{c}{2}U_P\ \overset{*}{\alpha} + \frac{C_{D0}}{a}U_T^2\right]\right.$$
$$+ \frac{2}{a}\left[U_T^2\Lambda f_1 + \frac{c}{4}U_T\ \overset{*}{\Lambda}\ f_2\right] - \frac{C_{D0}}{a}U_T U_P - \frac{2}{a}(\theta+\phi)\left[U_T U_P \Lambda f_1 + \frac{c}{4}U_P\ \overset{*}{\Lambda}\ f_2\right]$$
$$\left. - \frac{c}{2a}\left[U_T\ \overset{*}{\Lambda}\ f_3 + \frac{c}{2}\ \overset{**}{\Lambda}\ f_4\right]\right\} \tag{19}$$

$$M_\phi = \frac{\gamma}{6}\frac{c}{4}\left\{\frac{c}{4}\left[\overset{*}{U_P} - U_T\ \overset{*}{\alpha} - \frac{3c}{8}\ \overset{**}{\alpha}\right] - \frac{1}{a}\left[2U_T^2\Lambda(f_1+f_3) + \frac{c^2}{2}\ \overset{**}{\Lambda}\ f_8\right.\right.$$
$$\left.\left. + c\ U_T\ \overset{*}{\Lambda}\left(\frac{f_2}{2} + f_7\right)\right]\right\} \tag{20}$$

III. Solution Method

Several methods have been developed for the solution of nonlinear coupled partial differential equations representing the flap-lag-torsion motions of hingeless and bearingless rotor blades. A conditionally stable, explicit finite difference scheme to numerically integrate the nonlinear partial differential equations in space and time to obtain the aeroelastic response of elastic rotor blades has been introduced in references [14]. An identical numerical formulation is also used to obtain the transient and steady response of elastic hingeless rotor blades with flap control inputs.

For purposes of numerical integration by the proposed approach which is based on explicit finite difference methods, it is convenient to express the coupled nonlinear partial differential equations of rotor blade system in terms of first order time and second order space derivatives. This reduction is performed by introducing the following variables.

$$v_t = \overset{*}{\bar{v}}, \quad w_t = \overset{*}{\bar{w}}, \quad \phi_t = \overset{*}{\bar{\phi}} \tag{21}$$

and

$$m_v = \bar{v}^{++}, \quad m_w = \bar{w}^{++} \tag{22}$$

similary,

$$\overset{*}{m_v} = v_t^{++}, \quad \overset{*}{m_w} = w_t^{++} \tag{23}$$

where $()^*$ and $()^+$ are the partial derivatives with respect to nondimensional time variable, ψ, azimuth angle, and nondimentional spanwise location variable, $\bar{x}$, respectively. In terms of these variables, rotor blade nonlinear, coupled partial differential equations and

the trailing terms given in reference [13] are reorganized in reference [14] matrix form as follows,

$$\begin{aligned}
\overset{*}{\mathbf{u}}_t &= \bar{\mathbf{A}}(\mathbf{u},\psi)\mathbf{u}_m^{++} + \bar{\mathbf{B}}(\mathbf{u},\psi)\mathbf{u}_d^{++} + \bar{\mathbf{C}}(\mathbf{u},\psi)\mathbf{u}_d^{+} + \bar{\mathbf{D}}\mathbf{u}_t \\
&\quad + \bar{\mathbf{E}}(\mathbf{u},\psi)\mathbf{u}_m + \bar{\mathbf{F}}(\psi)\mathbf{u}_d + \bar{\mathbf{g}}(\mathbf{u},\psi) \\
\overset{*}{\mathbf{u}}_m &= \mathbf{I}_{23}\mathbf{u}_t^{++} \\
\overset{*}{\mathbf{u}}_d &= \mathbf{I}_{33}\mathbf{u}_t
\end{aligned} \tag{24}$$

where $\mathbf{u}_d$ and $\mathbf{u}_t$ are displacement and velocity vectors respectively and the matrices $\bar{\mathbf{A}}, \bar{\mathbf{B}}, \ldots, \bar{\mathbf{F}}$ and $\bar{\mathbf{g}}$ are given in reference [14].. The quantity $\mathbf{u}_m$ is vector defined in the following set of equations.

$$\mathbf{u}_t = \{v_t, w_t, \phi_t\}^T \quad , \quad \mathbf{u}_m = \{m_v, m_w\}^T \quad , \quad \mathbf{u}_d = \left\{\bar{v}, \bar{w}, \bar{\phi}\right\}^T \tag{25}$$

The vectors $\mathbf{u}_d$, $\mathbf{u}_t$ and $\mathbf{u}_m$ can be combined into a vector $\mathbf{u}$ as

$$\mathbf{u} = \{\mathbf{u}_t, \mathbf{u}_m, \mathbf{u}_d\}^T$$

The boundary conditions for the hingeless blade root at $\bar{x} = 0$

$$\mathbf{u}_d = 0, \quad \bar{v}^+ = 0, \quad \bar{w}^+ = 0 \tag{26}$$

Besides, the boundary conditions for blade tip at $\bar{x} = 1$ are $\phi^+ = 0$ at $\bar{x} = 1$ and

$$\mathbf{A}_{BC_m}\mathbf{u}_{m_m} = 0 \quad , \quad \mathbf{A}_{BC_m}\mathbf{u}_{m_m}^{+} = \mathbf{k}_I \tag{27}$$

$$\mathbf{k}_I = -\left\{ \begin{array}{c} 2\bar{m}\,\overset{*}{\theta}\,(\bar{k}_{m_1}^2 - \bar{k}_{m_2}^2)\sin\theta\cos\theta \\ 2\bar{m}\,\overset{*}{\theta}\,(\bar{k}_{m_2}^2\sin^2\theta + \bar{k}_{m_1}^2\cos^2\theta) \end{array} \right\}$$

where matrix $\mathbf{A}_{BC_m}$ is defined as

$$\mathbf{A}_{BC_m} = \left[\begin{array}{cc} B_{22} - \phi_m B_{23} & \frac{1}{2}B_{23} + \phi_m B_{32} \\ \frac{1}{2}B_{23} + \phi_m B_{32} & B_{33} + \phi_m B_{23} \end{array} \right]$$

$\mathbf{I}_{33}$ is a 3×3 identity matrix and matrix $\mathbf{I}_{2,3}$, is

$$\mathbf{I}_{2,3} = \left[\begin{array}{ccc} 1 & 0 & 0 \\ 0 & 1 & 0 \end{array} \right]$$

$\mathbf{I}_{33}$ is a 3×3 identity matrix.

The Explicit Finite Difference Approach

Finite difference approximations for rotor blade equations can be formulated in different ways. For time derivatives, the exact solutions of the rotor blade partial differential equations 24 $\mathbf{u}_{t_i}^{j+1}$ the node point $(\bar{x}_i, \psi_j + \Delta\psi)$ can be expanded in Taylor series as

$$\mathbf{u}_{t_i}^{j+1} = \mathbf{u}_{t_i}^{j} + \Delta\psi\mathbf{u}_{t_i}^{j^*} + \frac{1}{2}\Delta\psi^2\mathbf{u}_{t_i}^{j^{**}} + O(\Delta\psi^3) \tag{28}$$

Vectors $\mathbf{q}_{t_i}^j, \mathbf{q}_{m_i}^j$ and $\mathbf{q}_{d_i}^j$ are defined as approximations for $\mathbf{u}_t, \mathbf{u}_m$ and $\mathbf{u}_d$ at mesh point $(\bar{x}_i, \psi_{j+1})$ when only terms of the order of $\delta\psi$ are retained. Then, they can be combined into a vector $\mathbf{q}_i^j$ as

$$\mathbf{q}_i^j = \left\{ \mathbf{q}_{t_i}^j,\ \mathbf{q}_{m_i}^j,\ \mathbf{q}_{d_i}^j \right\}^T$$

With these approximations for time derivatives, a conditionally stable, explicit scheme can be introduced by using different azimuthal level substitution into equation 24. This scheme can be written as, at $(i, j+1)^{th}$ mesh position in a matrix form as

$$\begin{aligned}
\mathbf{q}_{t_i}^{j+1} &= \mathbf{q}_{t_i}^j + \Delta\psi \left\{ \bar{\mathbf{A}}_i^j \delta^2 \mathbf{q}_{m_i}^j + \bar{\mathbf{B}}_i^j \delta^2 \mathbf{q}_{d_i}^j + \bar{\mathbf{C}}_i^j \delta \mathbf{q}_{d_i}^j + \bar{\mathbf{D}}_i^j \mathbf{q}_{t_i}^j + \bar{\mathbf{E}}_i^j \mathbf{q}_{m_i}^j \right. \\
&\quad \left. + \bar{\mathbf{F}}_i^j \mathbf{q}_{d_i}^j + \bar{\mathbf{g}}_i^j \right\} + O(\Delta\psi^2) \\
\mathbf{q}_{m_i}^{j+1} &= \mathbf{q}_{m_i}^j + \Delta\psi \mathbf{I}_{23} \delta^2 \mathbf{q}_{t_i}^{j+1} + O(\Delta\psi^2) \\
\mathbf{q}_{d_i}^{j+1} &= \mathbf{q}_{d_i}^j + \Delta\psi \mathbf{I}_{33} \mathbf{q}_{t_i}^{j+1} + O(\Delta\psi^2)
\end{aligned} \tag{29}$$

In equation 29, δ and δ^2 are first and second order approximations tor first and second spatial derivatives respectively. In order to obtain a finite difference approximations to spatial derivatives the region to be examined is covered by a rectilinear grid with sides parallel to the x-axis and ψ-axis, with $\Delta\psi$ being the grid spacing in the ψ direction. The x-axis is divided into equal grids with lines paralell to the ψ-axis with coordiates $x = x_i, i = 0, 2, \ldots, m$ where $x_0 = 0$ and $x_n = 1$. This forms a grid rectangular time finite elements in time and space. The mesh points (x, ψ) are given by $x = x_i$, $\psi = N\Delta\psi$, where N is number of time intervals and $x_0 = 0$, $m = 0$ is the origin of solution domain.

The currently calculated velocity vectors $\mathbf{q}_{t_i}^{j+1}$ are substituted into equation 29 to calculate defined variables $\mathbf{q}_{m_i}^{j+1}$. This procedure makes the overall solution of the set of finite difference equations stable. The equation 29 depend on velocity vector $\mathbf{q}_{d_i}^{j+1}$ and it has been observed that averaging the velocitites vector $\mathbf{q}_{t_i}^{j+1}$ and $\mathbf{q}_{t_i}^j$ to calculate displacements has a destabilizing effect on the general solution of the numerical scheme. Therefore, displacements are calculated without averaging the velocities. Second order accuracy is obtained for spatial derivatives by central differencing. The accuracy of displacements, velocities and are defined variables are still first order in time.

To complete the formulation of the problem, the trailing terms are also approximated by finite differences. The boundary conditions at $x = 0$ is rewritten as

$$\mathbf{q}_{t_0} = 0, \quad \mathbf{q}_{d_0} = 0, \quad \mathbf{q}_{m_0} = \frac{2}{\Delta x^2} \mathbf{I}_{23} \mathbf{q}_{d_1} \tag{30}$$

The first spatial derivative of $\mathbf{q}_m$ at $\bar{x} = 1$ can be approximated as third spatial derivative of nodal displacement vector $\mathbf{q}_d$ as

$$\begin{aligned}
\mathbf{q}_{m_m}^{+} &= \mathbf{A}_{BC}^{-1} \mathbf{k}_I = \bar{\mathbf{q}}_{d_m}^{+++} \\
\bar{\mathbf{q}}_{d_m}^{+++} &\approx \mathbf{I}_{23} (h_{-2} \mathbf{q}_{d_{m-2}} + h_{-1} \mathbf{q}_{d_{m-1}} + h_0 \mathbf{q}_{d_m} + h_1 \mathbf{q}_{d_{m+1}})
\end{aligned} \tag{31}$$

where

$$\bar{\mathbf{q}}_{d_m} = \mathbf{I}_{23} \mathbf{q}_{d_m}$$

Coefficients h_{-2}, h_{-1}, h_0 and h_1 are obtained for equal mesh sizes as

$$h_{-2} = \frac{-1}{\Delta\bar{x}^3} \ , \quad h_{-1} = \frac{3}{\Delta\bar{x}^3} \ , \quad h_0 = \frac{-3}{\Delta\bar{x}^3} \ , \quad h_1 = \frac{1}{\Delta\bar{x}^3}$$

The variable, $\mathbf{q}_{m_m}$ is also approximated as

$$\begin{aligned} \mathbf{q}_{m_m} &= \mathbf{q}_{d_m}^{++} \approx \beta_{-1}\bar{\mathbf{q}}_{d_{m-1}} + \beta_0\bar{\mathbf{q}}_{d_m} + \beta_1\bar{\mathbf{q}}_{d_{m+1}} \\ &= 0 \end{aligned} \tag{32}$$

Equation 32 introduce a fictitious node $m+1$ which does not have any physical meaning but is needed to approximate the second and third order spatial derivatives at $\bar{x}$.

Finally the complete boundary conditions can now be written for equal element size $\Delta\bar{x}$ as

$$\begin{aligned} \mathbf{q}_{m_m} &= 0 \\ \bar{\mathbf{q}}_{d_m} &= 2\bar{\mathbf{q}}_{d_{m-1}} - \bar{\mathbf{q}}_{d_{m-2}} + \Delta\bar{x}^3\mathbf{A}_{BC}^{-1}\mathbf{k}_I \\ \phi_m &= \frac{4}{3}\phi_{m-1} - \frac{1}{3}\phi_{m-2} \\ \mathbf{q}_{t_m}^{n+1} &= \frac{\mathbf{q}_{d_m}^{n+1} - \mathbf{q}_{d_m}^{n}}{\Delta\bar{x}} \end{aligned} \tag{33}$$

Details of the above described numerical scheme is given in reference [14].

IV. Results and Discussions

Since the objective of this study is to illustrate the application of introduced approximate method, certain simplifications are made. These simplifications can be outlined as;

- Uniform inflow conditions along the blade span is considered.
- Hub and tip loses are only included by reducing the blade chord dimension at root and tip of the blade.
- Reverse flow effects are not included.
- Structural and mass properties of the blade are also taken as uniform along the blade.
- All offsets from the elastic axis are assumed to be zero.

Basic vehicle and rotor blade configuration parameters for the considered 220 lb test in flight model helicopter are given in Table 1. Main rotor has radius R_{mr}=3.8 ft. with blade chord c=.36ft. Trailing edge flap has a rectangular shape with width c_f=0.36 c_{MR} and starting from $r = 0.2R_{MR}$ to $r = 0.95R_{MR}$. Rotor blade for $r > 0.25R_{MR}$ has assumed to have lift generating airfoil sections. If an average rectangular blade has been considered, the equivalent average blade chord would be c_{av}= 0.28 ft. For the forward flight condition, component of the rotor thrust maintaining the forward propulsion must overcome the vehicle overall drag. Fuselage drag and its variation with vehicle angle of attack α for the considered model helicopter is approximated as;

$$\frac{D}{q} = 0.6 - 0.4\alpha + 6.00\alpha^2.$$

General configuration of the selected test mode helicopter is shown in Figure 2 Vehicle trim and rotor response calculatons are initiated from zero forward speed and flight conditions are defined with advance ratio μ, rotor angular speed Ω for the pure helicopter forward flight conditions. Forward speed is increased from μ=0.0 to μ= 0.2 with $\Delta\mu$=.0125 increments where as rotor angular speed is kept constant at its maximum value, Ω = 180 rad/sec. At each flight interval change the flap controls are introduced by linear increments.

Blade stiffness parameters

$$\Lambda_1 = \frac{EI_y}{m\Omega^2 R^4}, \quad \Lambda_2 = \frac{EI_z}{m\Omega^2 R^4}, \quad \Lambda_t = \frac{GJ}{m\Omega^2 R^4}$$

are nondimensionalized with rotor angular speed, main rotor radius and blade mass per unit length and Λ_1 and Λ_2 represent blade nondimensional bending stiffnesses in flapping (out of rotation plane) and lead-lag (in rotation plane) directions respectively. Blade nondimensional torsional stiffness is also represented with Λ_t.

Since the major objective of this study was to develop a numerial tool for calculating response of hingeless elastic blades with contoured flap geometries Two rotor blade configurations with different properties are considered.

Selected blade stiffness parameters are given in Table ?. Case 1 represents relatively stiff in flapping and softer in plane (lead–lag) blade and Case 2 represents the opposite configuration. For the first case two different trailing edge flap controls applied with 1/rev and 2/rev variations. Figure 3 shows the blade and trailind edge geometry selected test model helicopter configuration.

Table 1 : Stop Rotor Blade and Vehicle Configuration Parameters for Flap-Lag-Torsion Motions in Forward Flight

Number of blades	$b = 2$
Main rotor radius	$R_{MR} = 3.8$ ft
Main rotor speed	$\Omega_{MR} = 180$ rad/sec
Main chord	c_{MR}= .36 ft
Flap width	$c_f = 0.333 c_{MR}$
Hub offsets	x_{cg}= 0.08 ft
	h=1.1 ft
Gross weight	W_g= 220 lb
Cross sectional inertias	$\left(\frac{k_A}{k_M}\right)^2 = 1.0$
	$\left(\frac{k_M}{R}\right) = .025$
	$\left(\frac{k_{m_1}}{k_{m_2}}\right) = 0.0$
Blade drag coefficient :	C_{D0}=0.01
Solidity ratio :	σ=0.066
Lock number :	γ=6.
2-D Lift curve slope :	$a = 2\pi$
Advance ratio	μ, variable
Blade rigid pitch	$\theta_{ri} = 0.16$ rad
Blade pretwist angle	θ_{tw} = -.04 rad

Table 2 : Elastic Blade Stiffness Parameters.

	Λ_1 *Flap*	Λ_2 *Lag*	Λ_t *Torsion*
CASE 1	0.240	0.0041	0.004
CASE 2	0.0041	0.24	0.004

Applied flap controls for 1/rev and 2/rev cases are compared in figure 4.a where the magnitute of the controls for the second harmonics found to be higher than controls with first harmonics. Rotor blade elastic tip responses are obtained as the time history blade elastic motion while forward flight conditions have gradually changed. For the soft in–plane configuration $\Lambda_2 = 0.0041$ blade tip response samples are presented for flight condition $\mu = 0.175$. Blade has shown transient tip lead–lag characterictics for two configurations while flap and elastic tip deflections have reached steady motion within 2–3 blade revolution after a new flight condition control input were applied. For different sinuzoidal flap surface contours are considered and surfaces are defined as

$$\Lambda(\xi, \psi) = \Lambda(\xi)\Lambda(\psi)$$

Four different surfaces are selected as $\Lambda_s = \sin\frac{\pi\xi}{L_f}, \sin\frac{2\pi\xi}{L_f}, \cos\frac{\pi\xi}{L_f} and \cos\frac{2\pi\xi}{L_f}$.

Blade elastic lead–lag tip displacements are illustrated in Figure 4.b and harmonic content and surface shape have affected blade lead–lag transient response. Lead–lag responses for flat flap wit 1/rev harmonics with tha configuration of $\sin 2\pi$ shaped 2/rev harmonics, differed both in harmonic contents as well as the magnitute. Higher harmonics and $\sin 2\pi$ shape flaps have shown a stabilizing effect for this specific blade stiffness configuration.

Blade flapping dynamics have reached steadyness for each control case and significant change has been observed again for 2/rev, $\sin 2\pi$ control combination as seen in Figure 4.c.

Elastic blade twist has been quite affected both by the applied harmonics and flap shapes as being the result of trailing edge flap motions. Servo–flap activated blade control has been applied by twist controlled blades as outlined in reference [1] and this set of examples shows the potential of flap controls including elastic blade twist changing blade section effective angle of attack distribution.

V. Conclusions and Remarks

Since the major objective of this study was to develop a numerical tool to calculate elastic blade response for rotor slowing down transition mode, a specific emphasis was not given for the search and design of a particular blade or helicopter configuration. A systematic study must be done for a clear understanding of the blade transition dynamics and for the proper selection of blade stiffness and mass properties for a stable flap controlled rotor blade configuration. The approximate trim formulation found to be efficient for overall performance evaluations and trim solutions obtained for torsionally stiff configurations are within the accuracy of conventional pitch control trim calculations.

The aerodynamic formulation for the unsteady oscillating rotor blade airfoil with trailing edge flap controls and conditionally stable explicit finite difference scheme is found to be an effective method for calculating response of flap controlled blades applied by

contoured flap surfaces. With the use of paralel computing hardware and software capabilities of today's computer technologies it is also believed that explicit finite difference method can be also developed further to be an efficient tool for dynamic simulation of advanced rotorcraft blades with High Harmonic Control and Individual Blade Control features.

Based on these observations, present study is planned to be extended as;

- Elastic trim formulations are needed for a better modeling of lift variations due to the elastic twist of the blade.
- Flight objective functions defining the required optimum flight conditions must be imposed to simulate automatic pilot flight.
- Modeling elastic blade as elastic beam and deformable continious flap surface (trailing edge).
- Designing a stable, practically applicable flap controlled rotor blade for wind tunnel and test–in–flight model helicopter.
- extending the present studyby introducing a laminated piezoelectric beam sensor/actuator model capable of sensing/actuating all the extensional, thickness, torsional, flexural as well as coupled motions of the blade, within the frame of theories due to Dökmeci [15, 16] and Librescu, Song and Rogers [17], and using this model
- Examining, in particular, the torsional motions of the blade (cf. [18, 19]).

References

1) Strehlow, H.; and Rapp, H.: "Smart materials for Helicopter Rotor Active Control", AGARD CP-531, April 1993.

2) Lemnios, A.Z.; and Jones, R.: "The Servo Flap- An Advanced Rotor Control System", Presented at the AHS Design Specialist Meeting on Vertical Lift Aircraft Design, San Francisco, California, 17-19 January 1990.

3) Phillips, N.B.; and Merkley, D.J.: " BHTI's Technical Assessment of Advanced Rotor and Control Concepts", Presented at the AHS Design Specialists' Meeting on Vertical Lift Aircraft Design, San Francisco, California, 17-19 January 1990.

4) Straub, F.K.; and Merkley, D.J.: " MDHC's Technical Assessment of Advanced Rotor and Control Concepts", Presented at the AHS Design Specialists' Meeting on Vertical Lift Aircraft Design, San Francisco, California, 17-19 January 1990.

5) Yillikci, Y.K.; Hanagud, S.V.; Schrage, D.P.; Higman, J.: " Aeroelastic Analysis of Rotor Blades With Flap Control", Presented at the 18th European Rotorcraft Forum, September 15-18 1992, Avignon, France.

6) Rutherford, J.W.; O'Rouke, M.J.; Lovenguth, M.A.; and Mitchell, C.A.: "Concept Assessment of Two High Speed Rotorcraft", Journal of Aircraft, Vol. 30, No:2, March-April 1993, pp 241-247.

7) Blanchette, B.M.: "Design and Construction of A Ship Launched VTOL Unmanned Air Vehicle, Thesis, Naval Postgraduate School, Monterey CA, June 1990.

8) Kisli, E.; Prasad, J.V.R.; Yillikci, Y.K.: "Conceptual Design of A Stopped Rotor With Flap Controls", Presented at the 18th European Rotorcraft Forum, September 15-18 1992, Avignon, France.

9) Yillikci, Y.K., Prasad, J.V.R., and Schrage, D.P.: "Blade Response Simulations of Flap Controlled Stopped Rotors", Forum Proceeding, AIAA International Powered Lift Conference, 1-3 December 1993, San Francisco, USA.

10) Johnson, W.: Helicopter Theory, ch.2 Princeton, 1980.

11) "Bishlinghoff, R.L.; Asley, H; Halfman, R.L.:Aeroelasticity, Addison Wesley Publishing Company, 1975.

12) Kaza, K.R.V.; and Kvaternik, R.G.: "Engineering Notes- Application of Unsteady Airfoil Theory to Rotary Wings", Journal of Aircraft, Vol. 18, N0. 7, 1981.

13) Taylor, D. J., "A Method for the Efficient Calculation of Elastic Rotor Blade Dynamic Response in Forward Flight ", Doctoral Dissertation, School of Aerospace Engineering , Georgia Institute of Technology, Atlanta, Georgia, March 1987.

14) Yillikci, Y.K.; and Hanagud, S.V.: "Finite Difference Techniques and Rotor Blade Aeroelastic Partial Differential Equations: An Explicit Time-Space Finite Element Approach For P.D.E.", Presented at the 15th European Rotorcraft Forum, September 12-15, 1989, Amsterdam, Netherlands.

15) Dökmeci, M.C., "A Theory of High Frequency Vibrations of Piezoelectric Crystal Bars", Int. J. Solids Structures, Vol. 10, No: 4, pp. 401–409, 1974

16) Dökmeci, M.C., "Nonlinear Electroelastic Equations of Wave Propagation and Vibrations in Quartz Bars", Proceedings of the 40th Annual Symposium on Frequency Control, pp. 168–178, IEEE, Newyork, 1986,; and also IEEE Trans. Ultrason. Ferroelec. Freq. Contr., Vol. UFFC–33,No: 6, pp. 783,1986.

17) Librescu,L.:Song,O.; and Rogers, C.A.: "Adaptive Vibrational Behavior of Cantilevered Structures Modelled as Composite Thin–Walled Beams", Int. J. Engng. Sci., Vol. 31, No: 5, pp. 775–792,1993.

18) Dökmeci, M.C., "Recent Progress in the Dynamic Applications of Piezoelectric Crystals", The Shock and Vibration Digest, Vol. 20, No: 2, pp. 3–20, 1988

19) Rao, S.S.; and Sunar, M.: " Piezoelectricity and Its Use in Disturbance Sensing and Control of Flexible Structures: A Survey", Appl. Mech. Rev., Vol. 47, No: 4, pp. 113–123, 1994

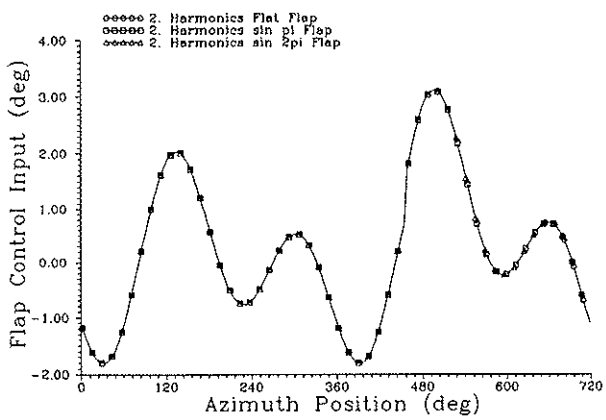

Figure 5.a Flap control inputs (Case 2).

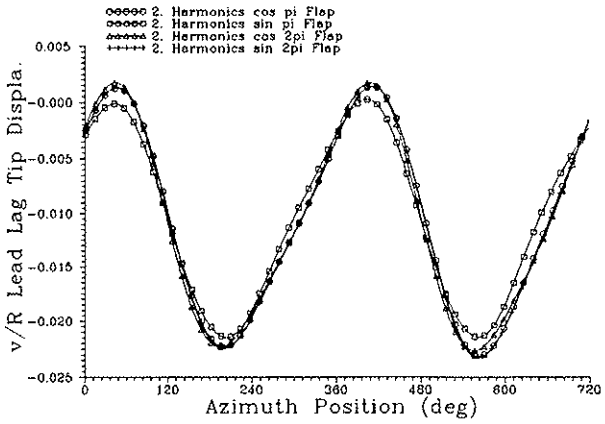

Figure 5.b Lead-lag tip deflections (Case 2).

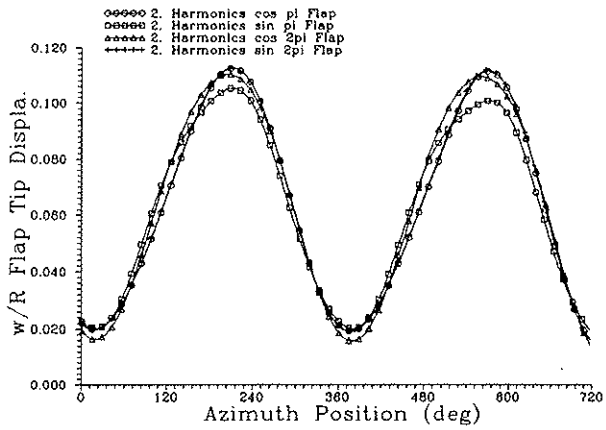

Figure 5.c Flap tip deflections (Case 2).

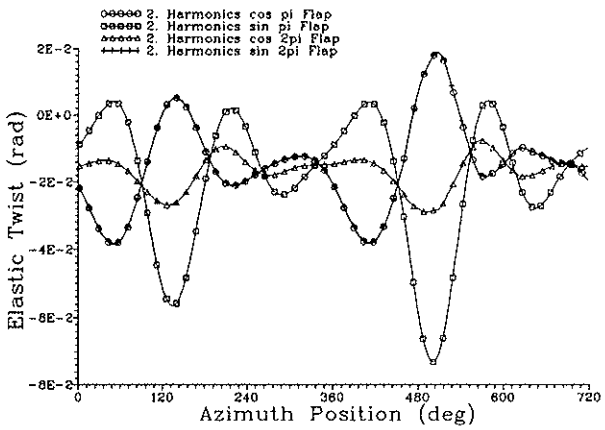

Figure 5.d Elastic twist (Case 2).

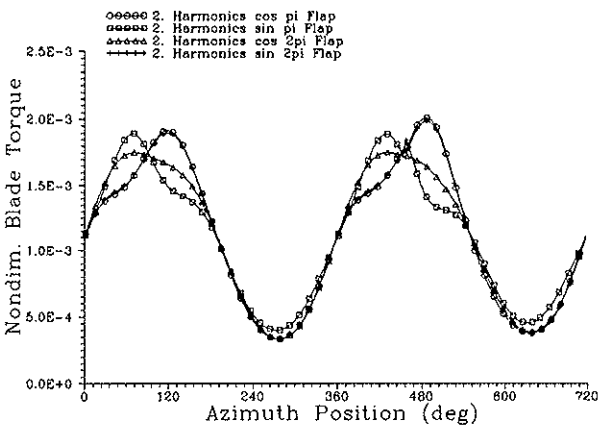

Figure 5.e Blade nondim. req. torque (Case 2).

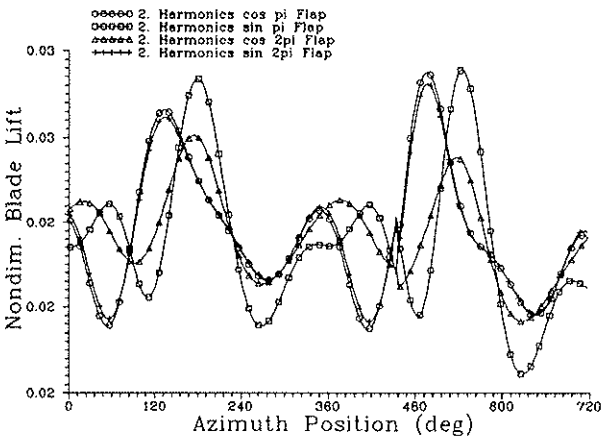

Figure 5.f Blade nondim. lift (Case 2).

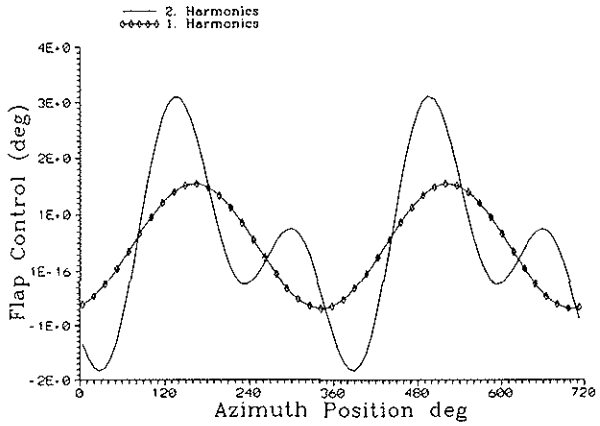

Figure 4.a Flap control inputs (Case 1).

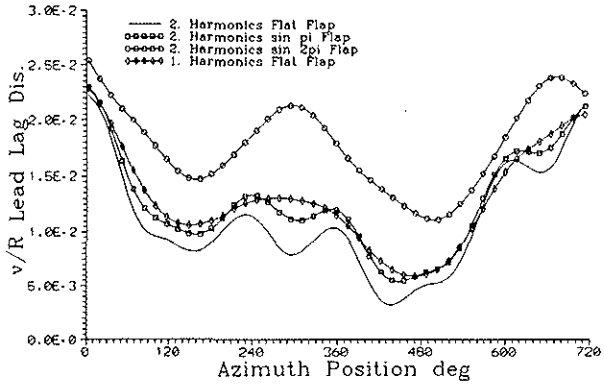

Figure 4.b Lead-lag tip deflections (Case 1).

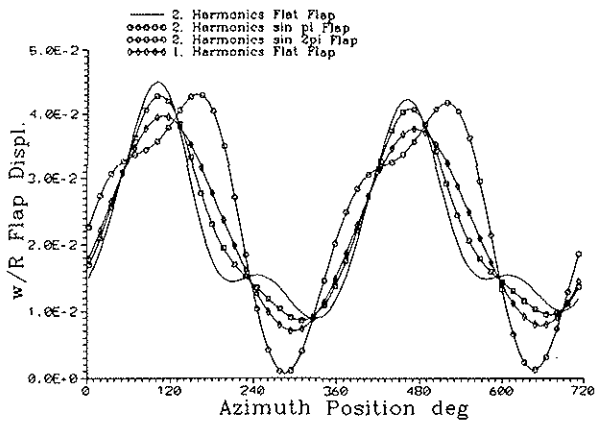

Figure 4.c Flap tip deflections (Case 1).

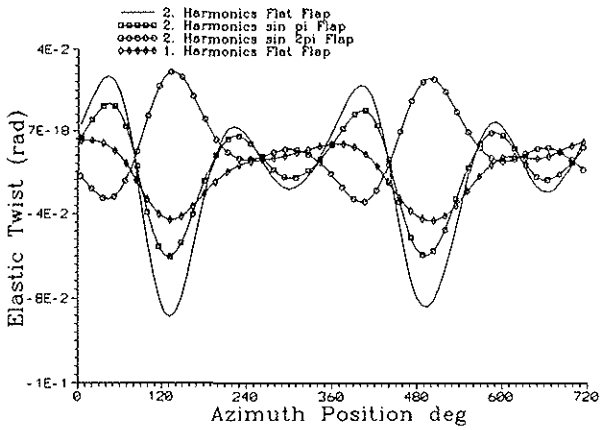

Figure 4.d Elastic twist (Case 1).

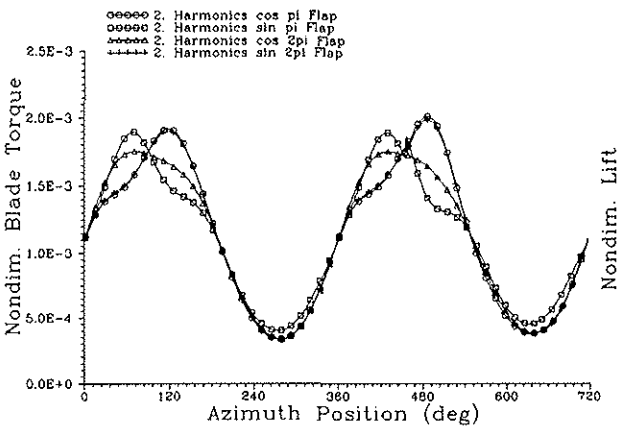

Figure 4.e Blade nondim. req. torque (Case 1).

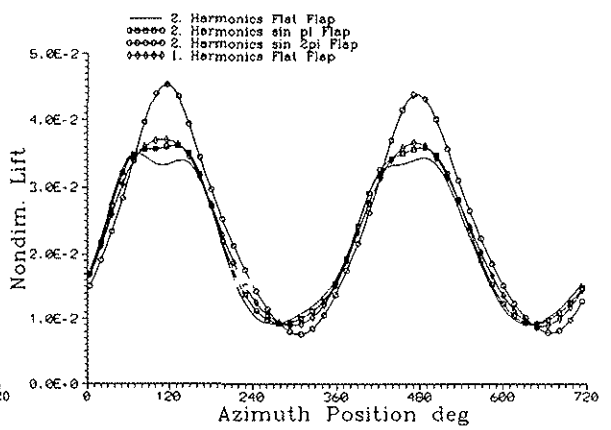

Figure 4.f Blade nondim. lift (Case 1).

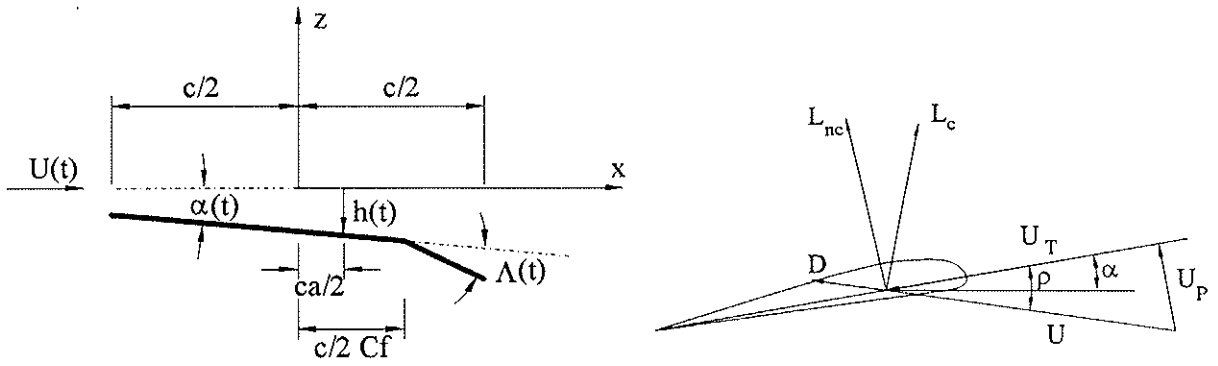

Figure 1 2-D Quisteady Blade Aerodynamics.

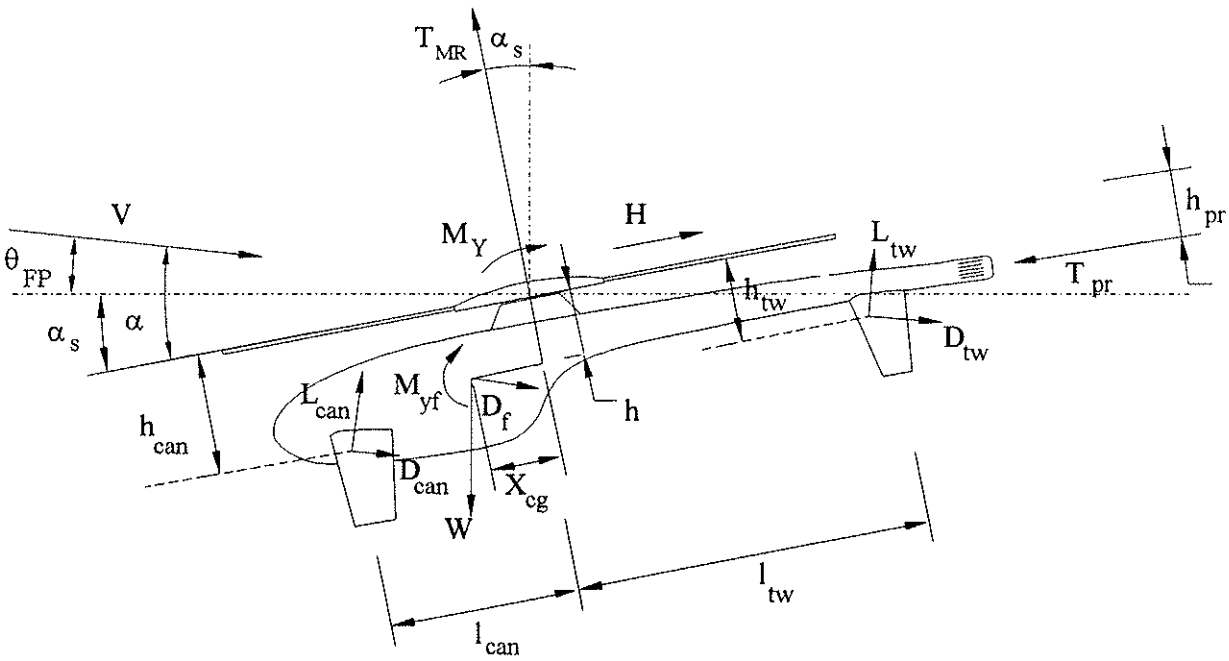

Figure 2 Test-in Flight Model Helicopter Configuration.

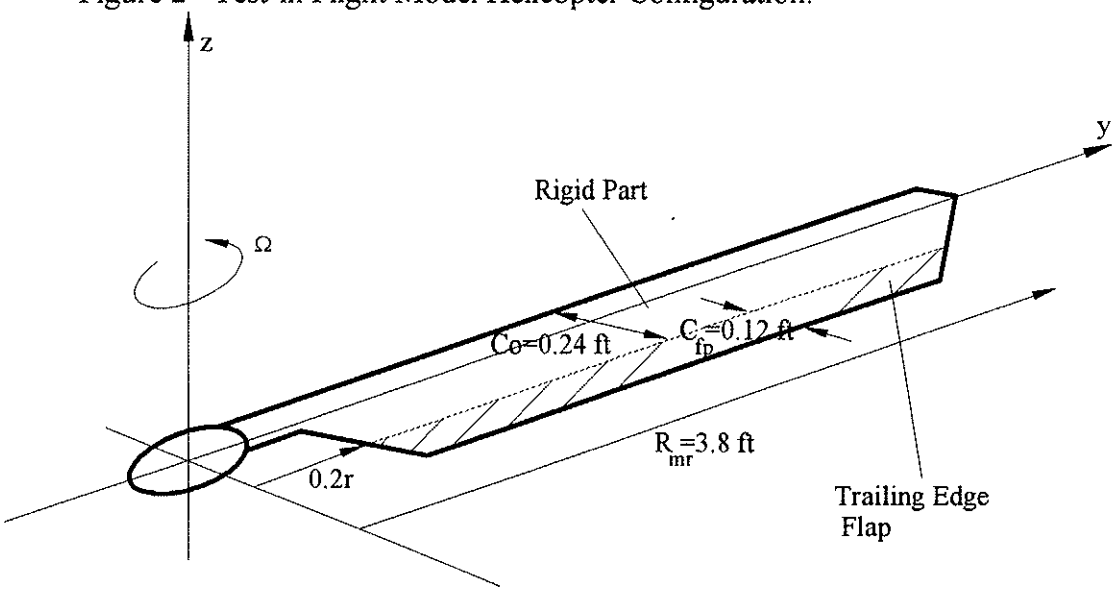

Figure 3 Flap Controlled Rotor Blade Configuration.